ARTICLE OPEN

Check for updates

Error measurements for a quantum annealer using the one-dimensional Ising model with twisted boundaries

Nicholas Chancellor[1,9]✉, Philip J. D. Crowley[1,10], Tanja Durić[1,11], Walter Vinci[1,12], Mohammad H. Amin[2,3], Andrew G. Green[1], Paul A. Warburton[1,4] and Gabriel Aeppli[5,6,7,8]✉

A finite length ferromagnetic chain with opposite spin polarization imposed at its two ends is one of the simplest frustrated spin models. In the clean classical limit the domain wall inserted on account of the boundary conditions resides with equal probability on any one of the bonds, and the degeneracy is precisely equal to the number of bonds. If quantum mechanics is introduced via a transverse field, the domain wall will behave as a particle in a box, and prefer to be nearer the middle of the chain rather than the ends. A simple characteristic of a real quantum annealer is therefore which of these limits obtains in practice. Here we have used the ferromagnetic chain with antiparallel boundary spins to test a real flux qubit quantum annealer and discover that contrary to both expectations, the domain walls found are non-uniformly distributed on account of effective random longitudinal fields present notwithstanding tuning carried out to zero out such fields when the couplings between qubits are nominally zero. We present a simple derivation of the form of the distribution function for the domain walls, and show also how the effect we have discovered can be used to determine the strength of the effective random fields (noise) characterizing the annealer. The noise measured in this fashion is smaller than what is seen during the single-qubit tuning process, but nonetheless qualitatively affects the outcome of the simulation performed by the annealer.

npj Quantum Information (2022)8:73 ; https://doi.org/10.1038/s41534-022-00580-w

INTRODUCTION

The low energy states of natural systems can correspond to the solutions of computationally difficult problems[1]. Experiments suggest that these low energy states can be accessed and measured by taking advantage of quantum mechanics, using a technique known as quantum annealing[2–4]. Here, the "difficult" problem is converted to an equivalent problem of finding the ground state of an Ising Hamiltonian, and that classical ground state is approached via the introduction and subsequent removal of quantum fluctuations, typically imposed via transverse fields. It is suspected but by no means universally agreed that quantum annealing could provide an improvement over other methods for certain classes of interesting problems[5,6]. To harness the power of quantum annealing, machines must be constructed to faithfully implement the relevant transverse field Ising Hamiltonian (TFIM), and to do so represents a major challenge in quantum information science and engineering. We refer to such machines as annealers. While the eventual outputs of annealers usually take discrete binary values, the control parameters, which are the coupling constants in the TFIM, must be chosen from a continuous set of values. An annealer should therefore be considered an analog rather than a digital computer. For a review of adiabatic quantum computing and quantum annealing see[7] and for a forward looking perspective on the field see[8].

Quantum annealing has attracted considerable experimental attention recently[9–16], which is understandable given the wide variety of applications, from traditional computer science problems[15,17], to more exotic uses such as aiding genetic algorithms to calculate radar waveforms[16], search engine ranking[18], graph isomorphism[13], and portfolio optimization[19]. In addition, sampling using a quantum annealer, which is effectively the topic of the current paper, is highly relevant to many machine learning and statistical inference tasks[20–26].

Precision of control parameters is a fundamental issue in analog computing, not present in its digital counterpart[27]. It is therefore important to ask what new complications these errors may add. One could hope, for example, that small uncorrelated control errors simply average out, leading to no noticeable effect as long as they are below a threshold[28]. Long time-scale noise should also be considered a source of control error; this noise will be indistinguishable from the TFIM being mis-specified by the device. We demonstrate here that the effects of control errors can be counter-intuitive, giving nonuniform distributions within a degenerate manifold even for uncorrelated errors. We further argue that this effect captures error-causing noise that would be missed if we try to measure the errors with a different protocol.

There is a growing literature on error correction in quantum annealing. Most of the studies focus upon the effect of coupling to an external bath rather than control errors[29–34]. The work in[28,35,36] does mention techniques that can reduce the effect of control errors, at the cost of some overhead, but cannot completely eliminate them. For the purposes of this study there are two kinds of relevant noise processes, the dissipation which occurs on a time scale comparable or faster than the system dynamics, and slower

[1]London Centre For Nanotechnology, University College London, London, UK. [2]D-Wave Systems Inc., Burnaby, BC, Canada. [3]Department of Physics, Simon Fraser University, Burnaby, BC, Canada. [4]Department of Electronic and Electrical Engineering, UCL, London, UK. [5]Physics Department, ETH Zürich, Zurich, Switzerland. [6]Institut de Physique, EPFL, Lausanne, Switzerland. [7]Paul Scherrer Institute, Villigen, Switzerland. [8]Quantum Center Eidgenössische Technische Hochschule Zurich, Zurich, Switzerland. [9]Present address: Department of Physics, Durham Newcastle Joint Quantum Centre, Durham University, Durham, UK. [10]Present address: Department of Physics, Massachusetts Institute of Technology, 182 Memorial Dr, Cambridge, MA 02142, USA. [11]Present address: School of Physical and Mathematical Sciences, Nanyang Technological University, 21 Nanyang Link, Singapore 637371, Singapore. [12]Present address: Quantum Artificial Intelligence Lab. (QuAIL), NASA Ames Research Center, Houston, TX, USA. ✉email: nicholas.chancellor@gmail.com; aepplig@ethz.ch

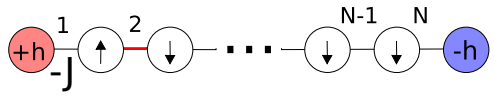

Fig. 1 Illustration of the Hamiltonian showing one of the ground states assuming that $h > J$ and the qubits at the ends satisfy the applied fields. Numbers indicate domain-wall sites.

noise which appears fixed with respect to these time scales and acts as effective random-field terms. The role of the faster noise is to hasten relaxation to a thermal distribution, while the slower noise (referred to as control errors) is what is directly measured in the experiments we report.

While the present study is dedicated to the consequences rather than the physical origins of the noise in flux qubit quantum annealers, we note other literature describing this noise as due to interactions of the qubit with magnetic defects in the chip substrate[37]. It typically takes a profile with a $\frac{1}{f}$ type frequency dependence, meaning that the noise contains both high and low frequency components. The low frequency components can be treated as effectively static control errors, and are responsible for the effects that we report here.

We examine experimentally the effect of control errors on the annealer constructed by D-Wave Systems, which mimics an Ising spin system. Our experiment shows a nonuniform distribution within a ground state manifold that can be explained by classical Boltzmann distributions under the influence of field control errors, demonstrating that even small errors affect the solution to strikingly simple problems. The fact that such a simple system subject to uniform noise can produce a nonuniform, but regular and predictable distribution, is an interesting mathematical result on its own, and to the best of our knowledge has not been previously reported in the literature.

We find that even a domain wall in a one-dimensional system subject to *uncorrelated* field control errors yields a nontrivial U-shaped domain-wall distribution. An effective potential for the domain walls is generated by combinatoric effects in the averaging over disorder in the Hamiltonian. In this sense the phenomenon that we observe is due to an entropic potential. While the average domain-wall energy is the same at every site; there are more field configurations where the lowest energy spin configuration has the domain wall near the ends, the probability of observing it in such positions is higher. This is a finite size effect distinguishable from order-by-disorder which occurs in infinite systems, where the term was originally used[38] to describe entropic effects in the thermodynamic limit. We further demonstrate that this distribution can be used to measure noise in the device and discuss the advantages over the conventional method of examining single-qubit autocorrelation.

The hardware that we use implements a transverse field Ising model with a time-dependent Hamiltonian of the form,

$$H(t) = -A(t)\sum_{i=1}\sigma_i^x + B(t)H_{\text{prob}}, \tag{1}$$

where H_{prob} is a user-specified Ising Hamiltonian, which is diagonal in the z basis, and $A(t)$, $B(t)$ are the annealing schedule, the time dependences that control the relative strength of each term.

The specific problem that we choose to study is a ferromagnetic chain with opposing fields at either end as shown in Fig. 1. As long as $|h| > J > 0$, H_{prob} will have an $(N-1)$-fold degenerate ground state manifold consisting of all states with a single-domain wall; $|\uparrow\downarrow\downarrow \ldots \downarrow\rangle$,$|\uparrow\uparrow\downarrow \ldots \downarrow\rangle \ldots$ $|\uparrow\uparrow \ldots \uparrow\downarrow\rangle$. This same system has been shown in[39,40] to be an effective method to encode discrete variables, and has been shown experimentally to improve performance in optimization[41,42]. In our experiments, we use $h = 2J$ with a Hamiltonian of the form

$$H_{\text{prob}} = J\sum_{i=1}^{N} -\sigma_i^z\sigma_{i+1}^z + h\left(\sigma_1^z - \sigma_{N+1}^z\right). \tag{2}$$

It is worth briefly noting that by keeping only the degenerate ground state subspace of Eq. 2, with the Hamiltonian in Eq. 1, we obtain a discretised particle-in-a-box Hamiltonian

$$H_{\text{deg}} = -A(t)\sum_{i=1}\left(a_i a_{i+1}^\dagger + a_i^\dagger a_{i+1}\right), \tag{3}$$

where a_i ($a_i^\dagger$) is an operator which annihilates (creates) a domain wall at location *i*. While in principle quantum effects within this manifold could be observed, we find that control errors dominate in our experiment.

We focus on control errors arising from stray magnetic fields from free spins and dangling bonds within the materials that make up the quantum processing unit (QPU). This could be considered equivalent to adding a term of the form,

$$H_{\text{fields}} = \sum_i \zeta_i\sigma_i^z, \tag{4}$$

to the overall Hamiltonian, where ζ_i are uncorrelated and Gaussianly distributed with a standard deviation $\sigma_\zeta \ll J$ and zero mean $\overline{\zeta_i} = 0$. The overline indicates an ensemble average. Random-field terms such as those in Eq. 4 appear naturally in implementations of the transverse field Ising model, including for example the dipole-coupled magnet $LiHo_xY_{1-x}F_4$[43]. Because the coupling between the qubits and the substrate is likely to change with bias, ζ_i will generally be time-dependent, however as we show later the system remains in thermal equilibrium until very late in the anneal, so it may be treated as static for the purpose of these experiments.

One can also consider coupler control errors of the form $H = \sum_i \zeta_i^{(J)}\sigma_i^z\sigma_{i+1}^z$, where $\zeta_i^{(J)}$ satisfy the same conditions as ζ_i with a standard deviation $\sigma_J \ll J$. This type of control error produces an uncorrelated potential for the domain walls, and therefore has no effect upon the shape of the mean thermal domain-wall distribution. We demonstrate this in Supplementary Section 2.1. It is worth noting briefly that[11] describes a similar experiment, but with the goal of demonstrating quantum tunneling, as had been done previously for a disordered magnet[44]. A qualitatively similar domain-wall distribution to the one that we see can be found in the Supplementary Material of ref. [11], although there is no discussion of this finding and its possible origins.

One concept that helps explain the behavior of these systems is *freeze time*, which is the time at which the dynamics of the QPU effectively stop and the spins are effectively fixed. Because the device appears to be reaching thermal equilibrium, we can think of these experiments as measuring the ratio of the noise level to the device temperature at the freeze time. Since the susceptibility of flux qubits to external noise will, in general, be different at different points in the experiment, the freeze time is an important (but not directly measurable) parameter.

Beyond control parameter errors, there is the quantum mechanical effect of zero point fluctuations which could be frozen out in a sufficiently fast read-out of the annealer; in the 1D problem considered by ourselves, the domain wall behaves as a "particle in a box" whose mass is regulated by the transverse field, implying a distribution of possible domain-wall positions with a peak in the middle of the chain, unlike the flat distribution expected for the ideal classical limit. Therefore, quantum fluctuations can cause quantum annealers to sample—in interesting ways—ground states unfairly[45–49], and such effects can sometimes be used in a beneficial way[50,51]). However, we conclusively demonstrate that the effect observed here is classical

in origin, both through numerical simulation and experiments using different runtimes. The reason that this system is dominated by classical rather than quantum effects is that it equilibrates quickly through thermal barrier hopping, as has been independently observed for one-dimensional chains in quantum annealers in[52].

RESULTS

Theoretical analysis

There is a vast literature on the one-dimensional Ising model dealing with issues ranging from random fields in the classical limit[53] through disordered couplers and transverse fields[54], to twisted boundary conditions in the clean quantum limit (see e.g., ref. [55]). Nonetheless, we could not locate a paper which specifically addresses the domain-wall distribution for the one-dimensional Ising model with twisted boundary conditions and a longitudinal random field, and what is relevant for quantum simulators, the evolution of this distribution with a transverse field. While such domain-wall distributions can be easily obtained through numerical sampling as we describe below, we provide in this section an analytical calculation in the classical limit, followed by some remarks on what could happen during the quantum annealing process.

Let us start by considering the energy contribution from the field control errors in the case of a single-domain wall on the nth coupler in the chain, $E_n = \sum_{i=1}^{N} sign(n - i + 0.5)\,\zeta_i$. The difference in energy between two domain-wall positions is therefore $E_n - E_m = 2\sum_{i=m+1}^{n}\zeta_i$ where $n > m$.

Assuming that $\overline{\zeta_i} = 0$ and $\overline{\zeta_i^2} = \overline{\zeta^2}$, we note that $\overline{E_n - E_m} = 2\sum_{i=m+1}^{n}\overline{\zeta_i} = 0$, but

$$\overline{(E_n - E_m)(E_n - E_k)} = 4\overline{\zeta^2}\min(|n-k|,|n-m|)\Theta[(n-k)(n-m)], \quad (5)$$

where Θ is a Heaviside theta. Note that this formula explicitly demonstrates that the domain-wall energies are correlated, even for uncorrelated fields. Also note that for a Gaussian distribution $\overline{\zeta^2} = \sigma_\zeta^2$. The probability of finding a domain wall at site n in a thermal ensemble averaged over noise is given by $P_n = \overline{Z^{-1}e^{-\beta E_n}} = \overline{\left[1 + \sum_{m\neq n} e^{-\beta(E_m - E_n)}\right]^{-1}}$.

Let us now consider a high-temperature approximation to obtain an analytical formula. By expanding this probability to second order in $\beta = \frac{1}{k_B T}$ and applying Eq. 5 we obtain

$$P_n \approx \tilde{P} + \beta^2\overline{\zeta^2}\frac{2}{N^2}\left(n - \frac{N+1}{2}\right)^2 \quad (6)$$

where $\tilde{P} = \frac{1}{N} - \frac{\beta^2}{N^3}\overline{\zeta^2}\left(\frac{5}{4}N^3 + N^2 + \frac{1}{6}N + 1\right)$. This demonstrates that even small field control errors create a parabolic (U-shaped) distribution of domain walls. Simple, uncorrelated errors can have a strong effect on the equilibrium behavior of a simple domain-wall system. Note that this calculation relies upon the assumption that the system is in thermal equilibrium. We justify this assumption numerically in Supplementary Section 2.2. We also demonstrate other derivations at finite and zero temperature in Supplementary Sections 2.3, 2.4. The expansion used in Eq. 6 is only guaranteed to be valid for temperatures much higher than the maximum difference in domain-wall energies, $\beta\zeta\sqrt{N} \ll 1$. We therefore expect that this approximation will breakdown for long chains, and experimentally demonstrate this breakdown in the paper. While the high-temperature expansion provides valuable intuition, we perform all analysis by comparing to computer aided numerical calculations.

The phenomenon of Eq. 6 is interesting as an experimental tool, because it provides a way of directly measuring the effect of the control errors on the evolution of a nontrivial Hamiltonian (i.e., with nonzero interactions between qubits). Therefore, we expect that the control errors measured in this way should give a more accurate portrayal of the errors experienced in a real computation than in single-qubit methods where interactions between qubits have been set to zero.

We conclude—to motivate future research—with considerations of what might happen during genuine ($T = 0$) quantum annealing and quenches. Most noteworthy is that for the twisted boundary conditions represented by Eqs. 1, 2, we have a domain wall which can be thought of as a particle whose mass approaches zero and size (uncertainty in position) diverges as the quantum critical point where A = J is approached (see ref. [44] and references therein). For a finite system, the wall is a particle in a box, which is more likely in its ground state to be found at the center of the box than at the edges. As we lower the transverse field below J, we expect the random fields to cause localization to occur as this is a one-dimensional system, i.e., in a chain of length L the domain wall should be localized as soon as its quantum mechanically defined size is smaller than L. What this means is that for a quantum annealer which is truly at zero temperature, the system can become trapped in a configuration which does not minimize energy. Furthermore, the random longitidinal fields would produce a distribution of wall positions (read out via projection of of individual spins onto the z axis) broader than expected for the clean limit.

Experimental results

Experiments were performed on a D-Wave Processor as described in "Methods" (and in more detail in the Supplementary Material), and we describe the key findings here. Firstly consider an individual instance of the Hamiltonian shown in Fig. 1 used in a quantum annealing protocol. Figure 2 demonstrates such an experiment, in particular annealing on the same chain run repeatedly over time with no averaging either over different definitions of 0 and 1 on the qubits (gauge averaging), or over different physical chains. As with most other experiments reported here each anneal took 20 μs. The distribution of domain walls is nonuniform, as expected for local random fields even though we have tuned the qubit controls in an effort to eliminate such random fields.

We now check whether the simple classical considerations of the previous section can account for our experimental observations. To avoid effects due to local variations in qubits and couplers, we average over different chains and gauges. Figure 2 also shows that the deviation between runs is much larger than expected for identical samples drawn from the same distribution, which can be seen by comparing the actual spread of the points

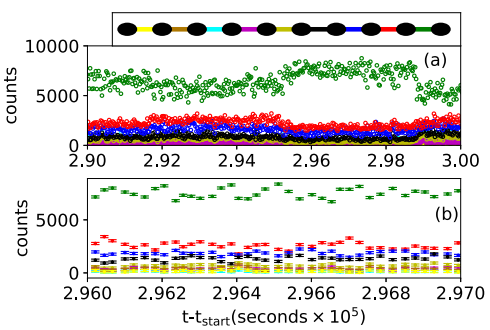

Fig. 2 Experimentally observed domain-wall counts for a single embedding and gauge choice versus sample time for a 10-qubit chain (domain wall sites are color coded in cartoon). Time scales are different for (**a**, **b**). Error bars in the bottom frame are standard error, and are suppressed in the top frame for clarity. Dashed lines in the top figure represent times when the system updates an internal self correction of biases.

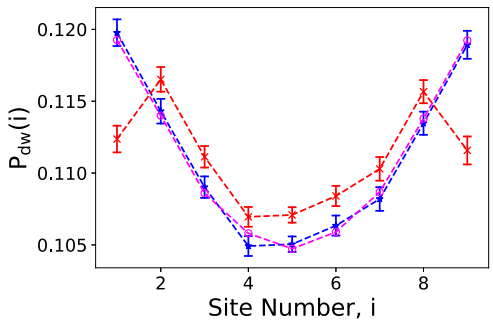

Fig. 3 Domain-wall probability distributions for 10-qubit frustrated chain. Crosses are raw experimental data. Asterisks are the same with a correction applied for background susceptibility. Circles are numerically calculated data from sampling Boltzmann distributions with field noise of the form Eq. 4 with $\frac{\sigma_\zeta}{T} = 0.2363$. Lines joining points are a guide to the eye.

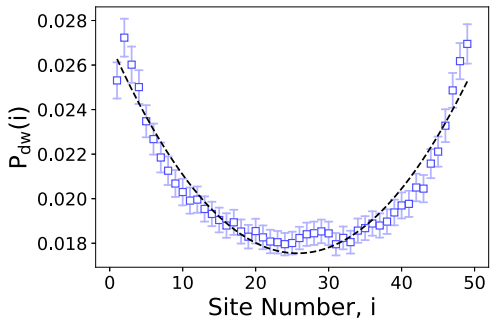

Fig. 4 Domain-wall distribution for a 50-qubit chain using the same experimental setup as Fig. 3 (including background susceptibility corrections). Dashed line is a parabolic fit. Error bars represent standard error.

with the standard error depicted in the error bars in the lower frame. This indicates that the control error has components that are faster than the time between samples. Fast errors are more difficult to detect, as well as to remove. For more discussion on this subject, see Supplementary Section 2.6.

The difference in domain-wall probabilities in Fig. 2 is due to a combination of control errors, of the form given in Eq. 4, and coupler control errors. However, as we described in Supplementary Section 2.1, measuring the average domain-wall distribution removes the effect of coupler errors, allowing us to measure only the field errors.

Figure 3 displays the results from running the QPU with the final Hamiltonian corresponding to the chain configuration shown in Fig. 1, while averaging over many embedding and gauge choices. An embedding corresponds to mapping a problem on a QPU such that every variable of the problem is represented by a subset of the qubits on the QPU. Note that chains can always be embedded in a one-to-one fashion, where every logical variable corresponds to one physical qubit; this is not true for more complicated graphs for which embedding is a more involved process[56]. Gauge choices arise due to an invariance of the target Hamiltonian under flips in the sign of a particular spin and the corresponding local field and couplings between it and other spins. This averaging is explained in the "Methods" section and Supplementary Section 1.1.

The experiment now yields a U-shaped distribution, with the probability for the domain wall to be located at the very end of the chain suppressed. The suppression is predicted from well understood rf-SQUID background susceptibility effects[57], and can be removed by applying a simple linear correction; for more details see Supplementary Section 1.2. Figure 4 shows the

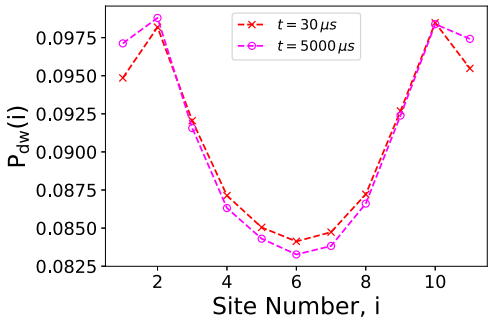

Fig. 5 Domain-wall distribution for a 12 qubit chain with two different anneal times. Standard error error bars are smaller than the depicted symbols. Background susceptibility corrections are not included.

behavior of the experiments when performed on a longer chain, where the distribution deviates from parabolic due to the breakdown of the assumptions underlying Eq. 6. For longer chains it is natural to ask whether Griffiths-McCoy-Wu singularities may be playing a role in the dynamics (such effects have recently been observed in two dimensional systems using quantum annealers[58]). However, these would manifest themselves as unusual configurations such as multiple domain walls with regular spacings between them, rather than the distribution of single-domain walls present in the ground state of a frustrated chain. In our experiments we predominantly observed the single-domain-wall state indicating that these effects were not playing a crucial role.

Although the theoretical predictions provide a good fit to the data, it is important to establish whether we are really justified in treating the output as a classical thermal distribution, and whether any residual quantum effects remain. It has been shown that performing quantum simulations on spin chain systems using D-Wave annealers is difficult due to the fact that a very fast quench is required to capture the dynamics. In fact simulations performed on unfrustrated spin chains in[52] suggest that a quench would need to be of order 10^5 times faster than currently available. As Supplementary Section 2.2 shows, we find the same result. The simulations in[52] also suggest that the scaling of the experiments is not favorable with system size, indicating that it will actually be more difficult to observe quantum effects in longer chains than the short ones we have simulated. To further confirm that the system is very close to thermal equilibrium, we perform annealing at two very different annealing times, as depicted in Fig. 5. In this figure we see that making the run time orders of magnitude longer makes only a small difference in that the minimum of the distribution is slightly more pronounced at longer runtimes.

We next examine the effect of the weak transverse fields which are still present at the freeze time, and whether this can lead to interesting quantum effects. We assume that the freezing occurs when $A(t) = 0.1\,GHz$, which is reasonable based upon previous work[11], and then compare the thermal distribution with or without the transverse field present, assuming a noise of $\frac{\sigma_\zeta}{T} = 0.24$ which can be extracted by fitting our experimental data as described later. Assuming a temperature of $T = 15\,mK = 0.31\,GHz$, we find the distributions in Fig. 6. The transverse field has very little effect, aside from a slight suppression of terminal site probabilities. We therefore conclude that the dominant effects observed in these experiments are indeed classical, and perform our remaining analysis from the perspective of classical thermodynamics.

Returning to analysis of the 10-qubit chain, the experimental data match the numerical data obtained by Boltzmann sampling over field noise of the type in Eq. 4 with $\frac{\sigma_\zeta}{T} = 0.24 (\sigma_\zeta \approx 0.074\,GHz)$. This fitting was performed against numerical sampling results rather than Eq. 6 to allow for higher-order corrections. Specifically, the

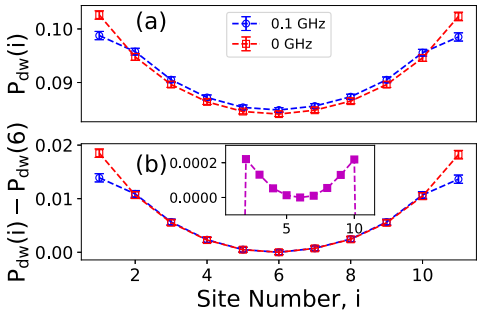

Fig. 6 Top: Numerically calculated domain-wall distribution assuming thermal equilibrium in the presence or absence of a transverse field for experimentally realistic parameters. Bottom: same as top but with mid-point value subtracted to allow direct comparison, inset is difference between the two curves. Both data were taken using the same 10^5 random noise realizations. Error bars are standard error, and this plot uses experimentally realistic parameters $\frac{\sigma_\zeta}{T} = 0.24$ and $T = 15\,mK = 0.31\,GHz$.

Table 1. Summary of different noise measurement techniques and the results obtained from them.

Measurement technique	Coupling on?	Sensitive to minimum time scale	$\frac{\sigma_\zeta}{T}$	σ_ζ(GHz)
Domain wall	Yes	N/A	0.2363	0.074
Naive sampling	No	1 s	0.13	0.040
Fourier transform	No	178 μs	0.35	0.11

fitting was performed by numerically sampling over disorder realizations and varying the parameter $\frac{\sigma_\zeta}{T}$ until the least squares error with respect to the experimental distribution was minimized. By contrast, a naive estimate made by sampling uncoupled qubit polarization yields $\frac{\sigma_\zeta}{T} = 0.13 (\sigma_\zeta \approx 0.040\,GHz)$.

The result that a naive single decoupled qubit measure of local random fields is substantially below the random fields needed to generate the nontrivial "U" distribution of domain walls for coupled qubits is a key outcome of our study. One possible explanation is that each sample is averaged over many annealing runs (each of which use the same annealing time as the domain wall experiments) and is therefore blind to any errors with a time-scale less than the time to collect all the samples, which is ~1 s. A more sophisticated analysis based upon calculating autocorrelation via the Fourier transform (FT) of the single-qubit results yields $\frac{\sigma_\zeta}{T} = 0.35 (\sigma_\zeta \approx 0.11\,GHz)$ (see Supplementary Section 1.3 for details) and so together with the outcome of the polarization sampling technique, brackets the result obtained from the domain-wall distribution for the Ising model with interacting qubits. As with the polarization calculation, the FT experiments are performed with the coupling turned off. This method is expected to be sensitive to a wider bandwidth of errors than the naive measurement, but should still be blind to any noise faster than the Nyquist interval, which in this case is about 178 μs . A summary of the different noise measurements can be found in Table 1.

Autocorrelation (FT), which has the fastest time scale, measures more error than the domain-wall technique or longer term sampling, which means that there are short-term fluctuations in uncoupled qubits which do not matter when we are dealing with the coupled qubits in the domain-wall problem.

Methods based on measuring the U-shaped distribution can further be used to address questions about the source of the control error. For example, we can measure the coupling dependence of the field control error by fixing the gauge of the chain and averaging over only embeddings. With a fixed gauge,

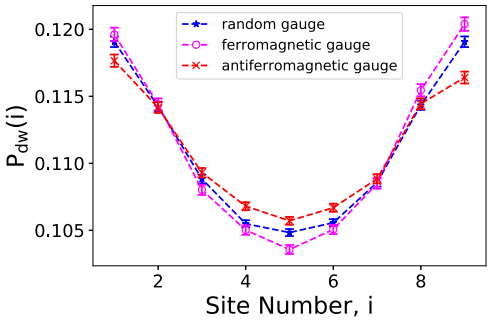

Fig. 7 Domain-wall distribution with different gauge choices. X represents data taken in the gauge which all couplers are antiferromagnetic. Asterisks are averaged over random gauges. Circles are data for the gauge in which all couplers are ferromagnetic. All data in this figure have been corrected for background susceptibility.

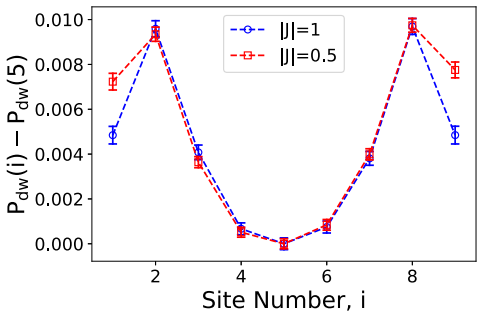

Fig. 8 Difference between domain-wall probability on site *i* from the probability that domain wall is found on site 5 for two scales of the coupling. Note that background susceptibility corrections have not been performed.

we must use a different embedding strategy to reduce correlations in the control errors caused by embedding to qubits in the same unit cell, see Supplementary Section 1.1. As Fig. 7 demonstrates, the depth of the U is different depending upon the gauge, which represents strong evidence that how the couplers are set influences the local random fields. This result is consistent with measurements performed by others that indicate that ferromagnetic couplers should couple more strongly to noise[59]. Our method of measuring the coupler-dependent portion of the control error does not require operation of the control lines outside of the preprogrammed annealing schedule of the device, while the method employed by[59] does.

For the U-shaped distribution to be useful to measure field control errors requires the underlying assumption that the errors are uncorrelated. Most types of correlation between nearby qubits will be removed by the process of gauge averaging. However, coupler-mediated errors from a shared coupler may depend on the state (ferro or anti-ferro) of the coupler[59], and therefore may contain some correlations that survive gauge averaging. We suspect that this part of the error should be relatively small because these correlations will only come from one of the 5 or 6 couplers connected to a given qubit, and only a fraction of the error from each coupler is state dependent[59,60].

We also have checked experimentally whether state-dependent errors have a significant effect. Figure 8 demonstrates that the depth of the distribution does not change within statistical error when the strength of the coupling is reduced by a factor of 2. If there were a strong component of the control error which depended on the state of the couplers, we would expect a substantial difference between the depth of these two distributions. This result is consistent with the mild dependence of the outcomes on gauge choice, and reinforces the concept that

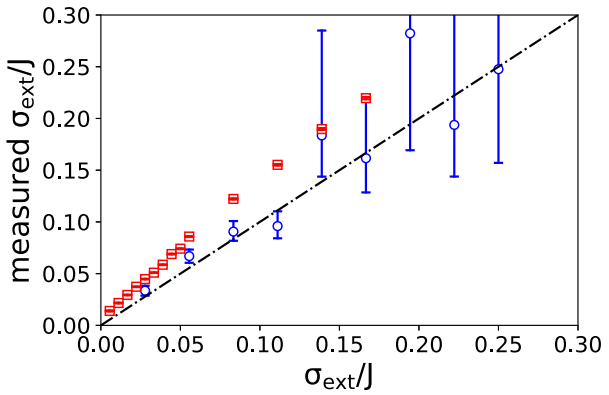

Fig. 9 Plot of measured values of σ_{ext}, where the local random fields measured in the absence of the imposed local fields σ_{ext}, are subtracted according to the quadrature formula in text, versus its actual value, assuming the system freezes when $A(t) = 0.1\,GHz$. The effective random-field strength we have used is the same as before, $\frac{\sigma_\zeta}{J} = 0.24$, so that T$= 15\,mK = 0.31\,GHz$ and $J = 1.80\,GHz$, we obtain $\frac{\sigma_\zeta}{J} = 0.041$. Blue circles are from comparing the "depth" of the U with numerical sampling. Red squares are from comparing autocorrelation with the results of numerical sampling. Dot-dashed line is a locus where measured and applied σ_{ext} are equal. For this plot we define the "depth" as the ratio of the probability to find the domain wall in the middle site over the sum of all probabilities excluding terminal sites. The terminal sites are excluded to avoid having to compensate for the background susceptibility effect seen in Fig. 3.

dynamical effects at the longest time and smallest energy scales are responsible for the discrepancies between the effective random fields seen for interacting and non-interacting qubits.

To validate the calibration of the random fields measured via the domain-wall technique relative to the single-qubit methods, we use the field controls of the chip to insert Gaussian control errors with a width σ_{ext}. Assuming that the original control error is not affected by the additional error that we insert artificially, the two errors will be independent, and the total error will be $\sigma_{tot} = \sqrt{\sigma_\zeta^2 + \sigma_{ext}^2}$. The strength of the inserted control errors, σ_{ext} is dependent on t, in the annealing schedule specified by $A(t)$ and $B(t)$ and therefore the time at which the qubits become effectively "frozen". It is important to note that σ_ζ can also depend upon the freeze time, so different freeze times with the couplings on versus off can potentially explain the deficit in the errors measured by the chain method. For our analysis we assume that the system freezes when $A(t) = 0.1\,GHz$, which is reasonable based upon previous work[11]. Figure 9 shows the measured value of σ_{ext} versus the programmed value. From this figure we see that within generous errors the domain-wall distributions agree with this model of the error, for which the results should appear on the diagonal indicated by the dashed blue line, while local autocorrelation measures an excess of error from the phenomenological result.

DISCUSSION

We consider the performance of a real annealer for one of the simplest illustrations of magnetic frustration, namely that of a magnetic domain wall in an Ising chain constrained to have opposite spin at either end. In the absence of random fields, the wall resides on any bond with equal probability. When quantum fluctuations are present, the wall behaves as a particle in a box, which is in its ground state will have maximum probability amplitude in the middle of the chain. On the other hand, when classical random fields dominate, the distribution function for the wall becomes "U" shaped, with a minimum at the middle of the chain. We demonstrate this result with a simple analytical calculation, and then proceed to observe that it is also the generic result for the D-Wave quantum annealer. Based on the fact that we see these effects even though local random fields are zeroed with couplings between qubits tuned to zero, new random fields may be induced when the couplers are turned on to implement interacting qubit Hamiltonians. Annealers are meant to solve optimization problems, e.g., in logistics or machine learning, with many degrees of freedom. The appearance of random fields as coupling terms are turned on after zeroing local random fields acting on individual qubits can produce the usual pathologies associated with random fields in statistical physics. Most notable among these are the pinning of "domain walls"[61,62]. The possibility that the couplings introduce noise should not come as a surprise given that we are after all, dealing with an analog computer. It is also not unprecedented in realizations of quantum annealers: for example, local longitudinal random fields can be induced by transverse fields in magnetic systems (see ref. [43] and references therein). We can turn a problematic but interesting effect (bug) into a benefit (feature) by using measurements of the "U" distribution to directly measure control errors for quantum annealers.

This method has several advantages which makes it a useful tool for understanding control errors in quantum annealing. It allows measurements to be made when couplers are active, therefore providing a more realistic estimate of the effects of control errors when solving real problems. Furthermore, the tests require no special access beyond the ability to submit problems to the device, so will be applicable for cases where users with limited access to the controls want to characterize noise in the controls. The relative ease of performing the measurements coupled with the fact that the measurements are performed in a fundamentally different way than the standard single, decoupled qubit measurements will also make running the 1D domain-wall problem a simple method for characterizing new devices. The errors detected for coupled qubits are important to characterize because it has been shown that if left unchecked, errors in the problem specification can have catastrophic effects on the result[63].

Our method runs with the standard annealing protocol, requiring no privileged access to the control lines, and measures the component of the noise which acts as control error *by construction*, with no frequency cutoff that depends on the annealing time. The second point means that the method could be used for arbitrarily long annealing times to observe deviations from the user-specified fields during the annealing process. On the other hand, should a processor be claimed to be a quantum simulator with a sufficiently rapid quench and read out, the domain-wall problem will yield a distribution with a maximum rather than minimum at the center of the chain, thus providing a qualitative test as to whether the device is classical random-field or quantum fluctuation- dominated. The cross-over between random field and quantum fluctuation-dominated regimes has been observed for model magnets[64], and we look forward to seeing a demonstration for properly programmable quantum simulators such as arrays of Josephson junctions or ion traps.

METHODS

Experimental methods

The data in all figures except Fig. 2 were taken on the USC Information Sciences Institute Vesuvius 6 D-Wave QPU. Except where otherwise stated, these data were averaged over gauges, as well as over ways of embedding on the QPU. For more details about the embedding see Supplementary Section 1.2. Data in Fig. 2 were taken using a QPU intermediate between the Vesuvius and Washington QPU generations made available by D-Wave Systems Inc. Unless otherwise stated all data were taken using an annealing time of 20 μs. All individual data sets are taken with 10,000 annealing runs.

DATA AVAILABILITY

The data and code are available from the authors upon request. Please contact Nicholas Chancellor at the email address provided with the author list.

Received: 14 October 2020; Accepted: 20 May 2022;
Published online: 27 June 2022

REFERENCES

1. Barahona, F. On the computational complexity of Ising spin glass models. *J. Phys. Math. Gen.* **15**, 3241–3253 (1982).
2. Kadowaki, T. & Nishimori, H. Quantum annealing in the transverse Ising model. *Phys. Rev. E* **58**, 5355 (1998).
3. Brooke, J., Bitko, D., Rosenbaum, T. F. & Aeppli, G. Quantum annealing of a disordered magnet. *Science* **284**, 779–781 (1999).
4. Santoro et al. Theory of quantum annealing of an Ising Spin Glass. *Science* **295**, 2427 (2002).
5. Farhi, E. et al. A quantum adiabatic evolution algorithm applied to random instances of an NP-complete problem. *Science* **292**, 472–475 (2001).
6. Hogg, T. Quantum search heuristics. *Phys. Rev. A* **61**, 052311 (2000).
7. Tameem, A. & Lidar, DanielA. Adiabatic quantum computation. *Rev. Mod. Phys.* **90**, 015002 (2018).
8. Hauke et al. Perspectives of quantum annealing: methods and implementations. *Rep. Prog. Phys.* **83**, 054401 (2020).
9. Boixo, S., Albash, T., Spaldalieri, F. M., Chancellor, N. & Lidar, D. A. Experimental signature of programmable quantum annealing. *Nat. Commun.* **4**, 3067 (2013).
10. Vinci, W., Albash, T., Mishra, A., Warburton, P. A. & Lidar, D. A. Distinguishing classical and quantum models for the D-Wave Device, Preprint at http://arXiv.org/abs/1403.4228 (2014).
11. Johnson, M. W. et al. Quantum annealing with manufactured spins. *Nature* **473**, 194–198 (2011). 12 May.
12. Boixo, S. et al. Quantum annealing with more than one hundred qubits. *Nat. Phys.* **10**, 218 (2014).
13. Vinci, W. et al. Hearing the shape of the Ising model with a programmable superconducting-flux annealer. *Sci. Rep.* **4**, 5703 (2014).
14. Harris, R. et al. Experimental investigation of an eight-qubit unit cell in a superconducting optimization processor. *Phys. Rev. B* **82**, 024511 (2010).
15. Santra, S., Quiroz, G., Ver Steeg, G. & Lidar, D. A. MAX 2-SAT with up to 108 qubits. *N. J. Phys.* **16**, 045006 (2014).
16. Coxson, G. E., Hill, C. R. & Russo, J. C. Adiabatic quantum computing for finding low-peak-sidelobe codes, IEEE High Performance Extreme Computing Conference (HPEC), pp. 1–6 https://doi.org/10.1109/HPEC.2014.7040953 (2014).
17. Choi, V. Adiabatic Quantum algorithms for the NP-Complete maximum-weight independent set, exact cover and 3SAT problems, Preprint at http://arXiv.org/abs/1004.2226 (2010).
18. Garnerone, S., Zanardi, P. & Lidar, D. A. Adiabatic quantum algorithm for search engine ranking. *Phys. Rev. Lett.* **108**, 230506 (2012).
19. Marzec, M. Portfolio Optimization: Applications in Quantum Computing, pages 73–106. (John Wiley & Sons, Inc., 2016).
20. Chancellor, N. et al. Maximum-entropy inference with a programmable annealer. *Sci. Rep.* **6**, 22318 (2016).
21. Amin, M. H., Andriyash, E., Rolfe, J., Kulchytskyy, B. & Melko, R. Quantum Boltzmann machine. *Phys. Rev. X* **8**, 021050 (2018).
22. Benedetti, M., Realpe-Gómez, J., Biswas, R. & Perdomo-Ortiz, A. Estimation of effective temperatures in quantum annealers for sampling applications: a case study with possible applications in deep learning. *Phys. Rev.* **A94**, 022308 (2016).
23. Benedetti, M., Realpe-Gómez, J., Biswas, R. & Perdomo-Ortiz, A. Quantum-assisted learning of graphical models with arbitrary pairwise connectivity. *Phys. Rev. X* **7**, 041052 (2017).
24. Khoshaman, A. et al. Quantum variational autoencoder. *Quantum Sci. Technol.* **4**, 014001 (2019).
25. Sadeghi, H. et al. PixelVAE++: improved PixelVAE with discrete prior, Preprint at http://arXiv.org/abs/1908.09948 (2019).
26. Winci, W. et al. A path towards quantum advantage in training deep generative models with quantum annealers. *Mach. Learn. Sci. Technol.* **1**, 045028 https://doi.org/10.1088/2632-2153/aba220 (2020).
27. Bissell, C.C. A great disappearing act: the electronic analogue computer. In: IEEE Conference on the History of Electronics, 28–30 (IEEE, 2004).
28. Young, K. C., Blume-Kohout, R. & Lidar, D. A. Adiabatic quantum optimization with the wrong Hamiltonian. *Phys. Rev. A* **88**, 062314 (2013).
29. Jordan, S. P., Farhi, E. & Shor, P. W. Error-correcting codes for adiabatic quantum computation. *Phys. Rev. A* **74**, 052322 (2006).
30. Lidar, D. A., Rezakhani, A. T. & Hamma, A. Adiabatic approximation with exponential accuracy for many-body systems and quantum computation. *J. Math. Phys.* **50**, 102106 (2009).
31. Lidar, D. A. Towards fault tolerant adiabatic quantum computation. *Phys. Rev. Lett.* **100**, 160506 (2008).
32. Young, K. C., Sarovar, M. & Blume-Kohut, R. Error suppression and error correction in adiabatic quantum computation: techniques and challenges. *Phys. Rev. X* **3**, 041013 (2013).
33. Quiroz, G. & Lidar, D. A. High-fidelity adiabatic quantum computation via dynamical decoupling. *Phys. Rev. A* **86**, 042333 (2012).
34. Ganti, A., Onunkwo, U. & Young, K. A family of [6k, 2k, 2] codes for practical, scalable adiabatic quantum computation. *Phys. Rev. A* **89**, 042313 (2014).
35. Pudenz, K. L., Albash, T. & Lidar, D. A. Error corrected quantum annealing with hundreds of qubits. *Nat. Commun.* **5**, 3243 (2014).
36. Matsuura, S., Nishimori, H., Vinci, W. & Lidar, D. A. Nested quantum annealing correction at finite temperature: p-spin models. *Phys. Rev. A* **99**, 062307 (2019).
37. Kumar, P. et al. Origin and Reduction of 1/f Magnetic Flux Noise in Superconducting Devices. *Phys. Rev. Appl.* **6**, 041001 (2016).
38. Villain, J., Bidaux, R., Carton, J.-P. & Conte, R. Order as an effect of disorder. *J. Phys. Fr.* **41**, 1263 (1980).
39. Chancellor, N. Domain wall encoding of discrete variables for quantum annealing and QAOA. *Quantum Sci. Technol.* **4**, 045004 (2019).
40. Abel, S., Chancellor, N. & Spannowsky, M. Quantum computing for quantum tunneling. *Phys. Rev. D.* **103**, 016008 (2021).
41. Chen, J., Stollenwerk, T. & Chancellor, N. Performance of Domain-Wall encoding for quantum annealing. *IEEE Trans. Quantum Eng.* **2**, 1–14 (2021). Art no. 3102714.
42. Berwald, J., Chancellor, N. & Dridi, R. Understanding domain-wall encoding theoretically and experimentally. Preprint at http://arXiv.org/abs/2108.12004 (2021).
43. Silevitch, D. et al. A ferromagnet in a continuously tunable random field. *Nature* **448**, 567–570 (2007).
44. Brooke, J., Rosenbaum, T. & Aeppli, G. Tunable quantum tunnelling of magnetic domain walls. *Nature* **413**, 610–613 (2001).
45. Matsuda, Y., Nishimori, H. & Katzgraber, H. G. Ground-state statistics from annealing algorithms: quantum versus classical approaches. *N. J. Phys.*, **11**, 073021 (2009).
46. Matsuda, Y., Nishimori, H. & Katzgraber, H. G. Quantum annealing for problems with ground-state degeneracy. *J. Phys.: Conf. Ser.* **143**, 012003 (2009).
47. Mandra, S., Zhu, Z. & Katzgraber, H. G. Exponentially biased ground-state sampling of quantum annealing machines with transverse-field driving Hamiltonians. *Phys. Rev. Lett.* **118**, 070502 (2017).
48. Könz, M. S., Mazzola, G., Ochoa, A. J., Katzgraber, H. G. & Troyer, M. Uncertain fate of fair sampling in quantum annealing. *Phys. Rev. A* **100**, 030303 (2019).
49. Kumar, V., Tomlin, C., Nehrkorn, C., O'Malley, D & Dulny, J. III. Achieving fair sampling in quantum annealing, Preprint at http://arXiv.org/abs/2007.08487 (2020).
50. Zhang, B. H. et al. Advantages of unfair quantum ground-state sampling. *Sci. Rep.* **7**, 1044 (2017).
51. Chancellor, N. Fluctuation-guided search in quantum annealing. *Phys. Rev. A* **102**, 062606 (2020).
52. Izquierdo, Z. G., Hen, I. & Albash, T. Testing a quantum annealer as a quantum thermal sampler. ACM Trans. Quant. Comput. **2**, 1–20 https://doi.org/10.1145/3464456 (2021).
53. Bruinsma, R. & Aeppli, G. One-dimensional Ising model in a random field. *Phys. Rev. Lett.* **50**, 1494 (1983).
54. Fisher, D. S. Critical behavior of random transverse-field Ising spin chains. *Phys. Rev. B* **51**, 6411 (1995).
55. Campostrini, M., Pelissetto, A. & Vicar, E. Quantum transitions driven by one-bond defects in quantum Ising rings. *Phys. Rev. E* **91**, 042123 (2015).
56. Fang, Y. & Warburton, P. A. Minimizing minor embedding energy: an application in quantum annealing. *Quantum Inf. Process* **19**, 191 (2020).
57. Harris, R. et al. *Phys. Rev. B* **81**, 134510 (2010).
58. Nishimura, K., Nishimori, H. & Katzgraber, H. G. Griffiths-McCoy singularity on the diluted Chimera graph: Monte Carlo simulations and experiments on quantum hardware. *Phys. Rev. A* **102**, 042403 (2020).
59. Trevor Lanting, D-Wave Systems Inc. private communication (2015).
60. Raymond, J., Yarkoni, S. & Andriyash, E. Global warming: temperature estimation in annealers. *Front. ICT* **3**, 23 (2016).
61. Bruinsma, R. & Aeppli, G. Interface motion and non-equilibrium properties of the random-field ising model. *Phys. Rev. Lett.* **52**, 1547 (1984).
62. Villain, J. Nonequilibrium "Critical" exponents in the random-field Ising model. *Phys. Rev. Lett.* **52**, 1543 (1984).
63. Pearson, A. et al. Analog errors in quantum annealing: doom and hope. *npj Quantum Inf.* **5**, 107 (2019).
64. Silevitch, D. M., Aeppli, G. & Rosenbaum, T. F. Switchable hardening of a ferromagnet at fixed temperature. *PNAS* **107**, 2797–2800 (2010).

ACKNOWLEDGEMENTS

The authors would like to thank Trevor Lanting, Murray Thom, Anatoly Smirnov, Stefan Zohren, and Jack Raymond for useful discussion. N.C. was supported by Lockheed Martin corporation and EPSRC fellowship EP/S00114X/1 while completing this work. T.D. was supported by EPSRC grant EP/K02163X/1. W.V. was supported by EPSRC grant EP/K004506/1. A.G.G. was supported by EPSRC grant EP/I004831/2. The authors thank the University of Southern California for allowing access to their D-Wave 2 quantum annealer as well as D-Wave Systems Inc. for access to the intermediate-generation annealer. Collaboration with USC is supported under EPSRC grant EP/K004506/1.

AUTHOR CONTRIBUTIONS

N.C. performed the experiments. M.H.A. and N.C. performed the calculations with useful assistance from A.G.G. M.H.A. produced the simulations which demonstrated that the system can be treated as equilibrated. N.C. wrote the paper. W.V. performed early experiments which demonstrated the effect. P.J.D.C. and T.D. performed simulations which informed the early directions of the project. A.G.G. recognized that the effect was related to order by disorder. N.C. and G.A. designed the experiment with P.A.W. providing a particularly useful suggestion. All authors were involved in discussions of the results.

COMPETING INTERESTS

The authors declare no competing interests.

ADDITIONAL INFORMATION

Supplementary information The online version contains supplementary material available at https://doi.org/10.1038/s41534-022-00580-w.

Correspondence and requests for materials should be addressed to Nicholas Chancellor or Gabriel Aeppli.

Reprints and permission information is available at http://www.nature.com/reprints

Publisher's note Springer Nature remains neutral with regard to jurisdictional claims in published maps and institutional affiliations.